INTERNATIONAL JOURNAL OF ENVIRONMENT, ENGINEERING & EDUCATION

ISSN 2656-8039 (ONLINE)
VOLUME 8 • ISSUE 1 • MARCH 2026

Received: 3 January 2026 | Accepted: 15 March 2026 | Published: 25 March 2026

Research Article

Effect of Vortex-Generator Planform and Height on the Trade-Off between Lift Enhancement and Wake Contraction around a Circular Cylinder

Karthik Jayanarasimhan [a,*] • Navin Kumar Balasubramanian [a] • Nagaraj Meenaskshi Sundaram [b]
M. Siva Sankari [c]

[a] Department of Mechanical Engineering, Saveetha School of Engineering, Saveetha Institute of Medical and Technical Sciences, Chennai, Tamil Nadu, India |
[b] Department of Agricultural Engineering, Saveetha School of Engineering, Saveetha Institute of Medical and Technical Sciences, Chennai, Tamil Nadu, India |
[c] Centre for Fluid Simulation, Rajalakshmi Institute of Technology, Chennai, Tamil Nadu, India

ABSTRACT

Passive flow control of circular-cylinder wakes remains important because wake organizations govern aerodynamic loading, force fluctuations, and vortex-induced response. This study examines how vortex-generator (VG) planform and height affect lift behavior and near-wake structure around a circular cylinder. Triangular and ogival VGs with heights of 4, 7, and 10 mm were mounted at the cylinder apex and evaluated using three-dimensional transient URANS simulations with the SST k–ω model at Re = 53,000. Supporting wind-tunnel force measurements were also performed to assess whether the numerical trends were qualitatively reproduced experimentally. All VG-equipped configurations reduced the recirculation region, narrowed the wake, and decreased the centerline velocity deficit relative to the clean cylinder. Among the triangular cases, the 10 mm VG produced the strongest wake contraction, reducing the recirculation length from 1.35D to 0.70D. Among the ogival cases, the 10 mm VG generated the highest peak lift coefficient (approximately 1.45), although its wake contraction remained slightly weaker than that of the corresponding triangular configuration. These results show that the geometry yielding the strongest wake suppression is not identical to that giving the highest lift enhancement. The wind-tunnel measurements reproduced the overall ranking trends. However, because the experimental inflow conditions were not Reynolds-number matched to the numerical setup, the comparison is interpreted as qualitative trend support rather than strict validation. The results demonstrate that the VG planform and height jointly control the trade-off between wake contraction and lift enhancement.

KEYWORDS aerodynamic performance • passive flow control • reynolds number • URANS simulations • wake control • wake topology • wind-tunnel experiment

ARTICLE CITATION

K. Jayanarasimhan, N. K. Balasubramanian, N. M. Sundaram, M. S. Sankari, "Effect of Vortex-Generator Planform and Height on the Trade-Off between Lift Enhancement and Wake Contraction around a Circular Cylinder," International Journal of Environment, Engineering and Education, Vol. 8, No. 1, pp. 122-137, 2026. https://doi.org/10.55151/ijeedu.v8i1.425

***CORRESPONDENCE**

Karthik Jayanarasimha karthikj9071.sse@saveetha.com Department of Mechanical Engineering, Saveetha School of Engineering, Saveetha Institute of Medical and Technical Sciences (SIMATS), Chennai, Tamil Nadu 602105, India. https://orcid.org/0000-0002-6294-0685

NOMENCLATURE

Symbol	Description	Symbol	Description
(V)	: Velocity	(Lr/D)	: Non-dimensional recirculation length
$(V_x), (V_y), (V_z)$	: Velocity along x, y, and z axes	$(a_1), (\beta^*), (\sigma_k), (\sigma_\omega)$	: Model constants
$(g_x), (g_y), (g_z)$	: Gravity along the x, y, and z axes	(φ)	: Position angle
(U_∞)	: Free-stream velocity	(δ)	: Boundary-layer thickness
$(U_{c(x)})$	: Centerline velocity	(ε)	: Dissipation
(D)	: Diameter of cylinder	(Λ)	: Maskell correction factor
(C_L)	: Lift coefficient	DPIV	: Digital Particle Image Velocimetry
$(C_{\{D,m\}})$	: Measured drag coefficient	CFL	: Courant-Friedrichs-Lewy
$(C_{\{D,\infty\}})$	: Corrected drag coefficient	CFD	: Computational Fluid Dynamics
$(h_{\{VG\}})$	: Height of vortex generator	VGs	: Vortex Generators
$(l_{\{VG\}})$	: Length of vortex generator	RANS	: Reynolds-Averaged Navier-Stokes equations
(k)	: Turbulent kinetic energy	SST	: Shear Stress Transport
$(F_1), (F_2)$	: Blending functions	SIMPLE	: Semi-Implicit Method for Pressure-Linked Equations
(P_k)	: Production of turbulent kinetic energy	FSP	: Flow Separation Point
(ω)	: Specific dissipation rate	VIV	: Vortex-Induced Vibration
(ρ)	: Density	LES	: Large Eddy Simulation
(μ_t)	: Turbulent viscosity	WT	: Wind tunnel
(f)	: Vortex shedding frequency	TI	: Turbulence Intensity
U_{rms}	: Root means square velocity	TNPESU	: Tamil Nadu Physical Education and Sports University

1. INTRODUCTION

Flow control has long been recognized as a fundamental strategy for regulating boundary-layer development, delaying flow separation, and modifying wake dynamics in both external and internal flows. Its importance stems from the strong influence of separation and wake formation on aerodynamic and hydrodynamic performance, including drag penalty, lift generation, fluctuating forces, pressure loss, heat-transfer characteristics, and flow-induced vibrations. In aerodynamic applications, effective flow-control strategies can improve lift [1], reduce drag [2], delay the onset of separation, and enhance flow mixing [3]. Consequently, flow control has become integral to a broad range of engineering systems, including aerospace configurations [4], [5], automotive bodies [6], turbomachinery components [7], [8], and biomedical flow devices [9], [10]. In addition to improving aerodynamic efficiency, flow control enhances thermal performance [11] and mitigates flow-induced noise in propulsion and acoustic systems [12].

More broadly, flow control seeks to manipulate momentum exchange within the boundary layer and separated shear layers to weaken or delay undesirable flow phenomena. In bluff-body flows, such phenomena typically include premature separation, large recirculation regions, intense vortex shedding, fluctuating lift forces, and elevated drag. These effects are particularly important because they directly affect structural loading, aeroacoustic emissions, and vortex-induced vibration (VIV). Accordingly, the ability to suppress or reorganize the wake has become a central topic in fluid mechanics, especially for canonical bluff-body configurations such as the circular cylinder. In this geometry, the interactions among separation, recirculation, and vortex shedding can be examined in a relatively simple configuration while preserving rich, practically relevant flow physics. The generic topology of separation and wake development around a circular cylinder (Figure 1).

Flow-control strategies for circular cylinders are generally classified as either active or passive. Active control requires external energy input, such as synthetic jets [15], plasma actuators [16], blowing, suction, or oscillatory forcing. It can provide strong control authority, albeit at the cost of greater system complexity. Passive control, by contrast, modifies the boundary layer and wake through geometric devices such as vortex generators [17], riblets [18], roughness elements, and splitter plates, making it simpler and often more practical for implementation.

Numerous studies have investigated flow control over circular cylinders to reduce flow separation, vortex shedding, drag, and vibration. Igarashi [19] showed that a slit can shift the vortex formation region downstream and suppress vortex shedding, whereas Shiels et al. [20] reported drag reduction under rotary oscillation. Lim and Lee [21] found that O-rings reduced drag by approximately 9%, and Wang and Zhao [22] showed that wake interaction with a wall boundary layer modifies the structure of the turbulent boundary layer. Using two-way fluid–structure interaction simulations, Izhar et al. [23] further demonstrated that vortex generators can suppress vortex-induced vibrations.

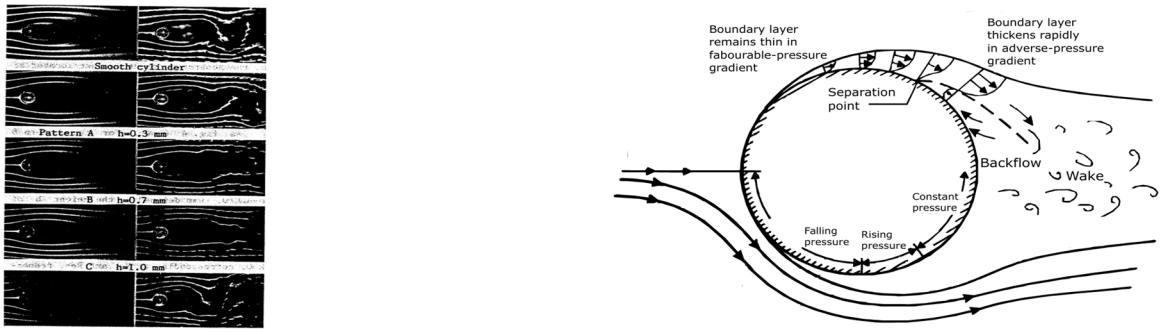

(a) (b)

Figure 1. Wake topology of flow over a circular cylinder: (a) flow visualization of a baseline cylinder and a cylinder equipped with vortex generators, adapted from Igarashi et al. [13]; (b) schematic of separation and near-wake development around a circular cylinder, adapted from Groh et al. [14].

More recent studies have revealed additional mechanisms for wake control. Yu et al. [24] showed that symmetric synthetic jets confine wake vorticity and reduce downstream velocity fluctuations, whereas Jiang [25] proposed an empirical relationship between the time-averaged separation angle and the Reynolds number. Soti and De [26] identified an optimal mass-damping value for maximizing power extraction, Chatzimanolakis [27] described the formation of secondary dipole-like vortices in impulsively started flow, Gong and Dally [28] examined the effects of plate insertion between tandem cylinders, and Li et al. [29] reported that V-riblets delayed separation and reduced drag by up to 6.81%.

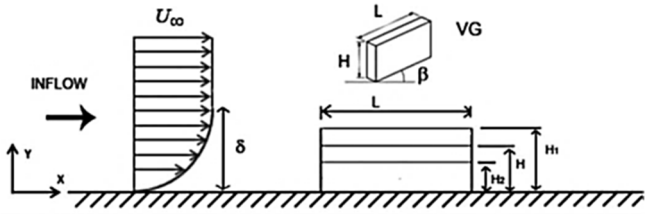

Figure 2. Operating principle and characteristic geometric parameters of a vortex generator [30].

Among passive flow-control devices, vortex generators (VGs) are particularly effective because they generate streamwise vortices that transport high-momentum fluid toward the wall. By energizing the boundary layer, they delay separation, narrow the wake, and weaken vortex shedding. The development of VGs can be traced from the early work of Taylor [31] and Gyatt [32] to the experimental observations of Kobayashi and Maekawa [33]. Subsequent studies demonstrated that fluidic and mechanical VGs influence vortex formation through different mechanisms [2], that VGs can shift separation downstream and improve wake structure [34], [35], and that their effectiveness depends strongly on geometry and placement [36]. Common VG profiles include triangular, vane, rectangular, gothic, ogival, and wishbone configurations. Among these, triangular VGs are attractive because of their geometric simplicity and effectiveness at low Reynolds numbers [37], whereas ogival VGs have also been applied in automotive and heat-exchanger systems [38], [39].

For circular cylinders in particular, recent studies have confirmed that VGs can substantially modify near-wake organization. Okbaz et al. [40] reported that appropriately oriented VGs elongated the wake, reduced velocity fluctuations, and decreased the drag coefficient by up to 35.3% relative to a bare cylinder. Similarly, Aksoy [41] showed experimentally that the position and yaw angle of triangular VGs significantly influence wake development around a circular cylinder at a Reynolds number of 8000. More recently, Wang et al. [42] demonstrated that nonconventional, nature-inspired vortex-generator geometries can also reorganize the wake, suggesting that VG planform shape should be treated as a primary design variable rather than a secondary geometric detail. Taken together, these findings indicate that VG performance is highly sensitive to both geometry and placement. Physically, VG height governs the depth to which the generated vortices penetrate the boundary layer. In contrast, VG profile influences vortex formation, parasitic losses, and the subsequent organization of the separated shear layers. A selective synthesis of representative studies on flow control over circular cylinders (Table 1).

Table 1. Summary of representative studies on flow control over circular cylinders.

Authors	Re (x10^5)	Method	Flow control	Dimensions	Observations
Okbaz et al. (2023) [40]		PIV	Triangular VG	Ω=30°; β=60°.	VGs elongated the wake and the vortex formation length, reducing velocity fluctuations.

Authors	Re (x10^5)	Method	Flow control	Dimensions	Observations
Igarashi (1986) [13]	0.13-0.52	Hot wire	Slit	s/d:0.08, 0.185 φ =0°-90°	The vortex region moves downstream, and the vortex shedding frequency decreases due to the slit.
Aksoy (2024) [41]	0.08	PIV	Triangular VG	Ω=15°,30°,60°,75°. β=30°,45°,60°,75°.	High-velocity fluctuations, turbulent intensities, and considerable drag reduction (~33.3%) are observed in a cylinder with VG.
Gardarin et al. (2008) [2]	4.0	WT testing	MVG, FVG	l_{VG}=1.8δ; h_{VG}=0.6δ ; φ =20°	Fluidic VG produced more vortices, and the vortex circulation produced by mechanical VG is 100% higher than that of fluidic VG.
Lim & Lee (2004) [21]	0.078-1.20	WT testing	O-rings	d=D/60, D/20, D/15	9% drag reduction is observed at d = D/60 compared to the smooth cylinder.
Unal & Atlar (2010) [34]	0.413	DPIV		h_{VG}/l_{VG}=0.5 s/h_{VG}=4.0; φ=+/- 10°	VGs enforced the shear layers, bringing them closer together and reducing the near-wake width, thereby increasing the mean circulation.
Muddada & Patnaik (2010) [43]	0.001-0.003	CFD, Flow visualization	Actuator	φ=120° {behind cylinder}	Vortex shedding suppression is observed at Re=100 and validated through flow visualization with tracer particles.
Schulmeister et al. (2017) [44]	0.47 (3D) 0.05 (2D)	Water tunnel, CFD & PIV	Counter-rotating cylinders	D=0.05m; L/D=9.8	Rotating cylinders narrow and stabilize the wake, thereby shortening the length of the recirculation region. Drag reduced by 45%
Jirasek (2005) [45]	3.9	CFD (jBAY)	Triangular VG	h=δ; x/c=25%	VGs reduce the recirculation zone and separation, giving high lift
Shur et al. (2015) [46]	5	CFD	Vane	h/δ=1,0.5,0.25 x/D=0.03,0.07	Counter-rotating arrangement of VGs with h/δ=0.5 performed better in drag reduction (~60%) and enhanced near-wall momentum.
Heine et al. (2018) [47]	2.2	WT testing, PIV	Leading edge VG	h=0.5mm, s=20mm φ =0°-90°	Bundles of wakes are visible at very low (6°-15°) and very high (78°-90°) inclinations. Flow separation is effective in 15°-78°
Matejka et al. (2009) [48]	0.69;1.93	WT testing	Synthetic jet slot	S = 275mm, t = 0.5mm φ = 90° & 100°	Flow control is efficient at low Re (69000) as the synthetic jet adds momentum to the laminar transition region and stabilizes the wake.

Despite extensive investigation of passive appendages for drag reduction and mitigation of vortex-induced vibrations in cylinder wakes, comparative evidence regarding the combined effects of vortex-generator planform and height on lift behavior and near-wake reorganization under matched test conditions remains limited. Previous studies have focused primarily on conventional triangular or vane-type devices and have generally emphasized drag-related outcomes rather than lift response and its relationship to separation topology.

Against this background, the present study investigates the influence of vortex-generator profile and height on the aerodynamic performance of a circular cylinder, with particular emphasis on the lift coefficient and wake dynamics. Two vortex-generator profiles, triangular and ogival, are examined at different heights under identical geometric and flow conditions. By integrating transient URANS simulations with wind-tunnel measurements, this study evaluates how vortex-generator geometry affects flow separation, recirculation, vortex shedding, and lift response. It identifies the configuration that provides the best flow-control performance under the current operating conditions.

2. MATERIALS AND METHODS

2.1. Geometric Modeling of Vortex Generators

In the present analysis, a pair of triangulars or ogival vortex generators (Figure 3) is positioned at the apex of the cylinder. The study combines numerical and experimental approaches to compare the effects of VG profile and height on wake development, vortex shedding, and lift response. The VG height is varied as h_{VG} = 4, 7, and 10 mm.

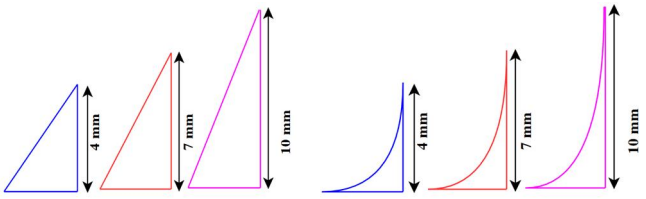

Figure 3. Conceptual Framework for AI-Powered Environmental Education

Air is used as the working fluid under standard laboratory conditions. Based on the literature, the inclination angle relative to the cylinder surface is fixed at 30°, and the

vortex generator length is set to 5 mm, corresponding to $l/D = 0.125$ for the cylinder diameter considered in the present study.

In the numerical study, the Reynolds number is fixed at 53,000 to enable comparison across the six VG configurations within a representative subcritical regime. The wind-tunnel measurements are used as supporting experimental evidence for the force-response trends. However, they should not be interpreted as a strict Reynolds-number-matched validation of every numerical result. The main objective of the study is therefore to compare the relative aerodynamic effects of triangular and ogival VGs, rather than to claim a universally optimized geometry.

2.2. Governing Equations

This study solves the three-dimensional, unsteady, incompressible Reynolds-averaged Navier-Stokes equations for air flow around the cylinder-VG configuration. The formulation assumes incompressible flow, no-slip and impermeable solid boundaries, and negligible gravitational effects. The governing system, therefore, consists of the continuity equation and the momentum equations in the streamwise, transverse, and spanwise directions. To close the RANS system, the shear stress transport (SST) k-omega turbulence model is employed via transport equations for the turbulent kinetic energy k and the specific dissipation rate omega.

The continuity equation is written as:

$$\frac{\partial}{\partial x}(\rho V_x) + \frac{\partial}{\partial y}(\rho V_y) + \frac{\partial}{\partial z}(\rho V_z) \tag{1}$$

The momentum equations in the x-, y-, and z- directions are expressed as:

$$\frac{\partial}{\partial x}(\rho V_x V_x) + \frac{\partial}{\partial y}(\rho V_y V_x) + \frac{\partial}{\partial z}(\rho V_z V_x) = \rho g_x - \frac{\partial P}{\partial x} + \frac{\partial}{\partial x}\left(\mu_e \frac{\partial V_x}{\partial x}\right) + \frac{\partial}{\partial y}\left(\mu_e \frac{\partial V_x}{\partial y}\right) + \frac{\partial}{\partial z}\left(\mu_e \frac{\partial V_x}{\partial z}\right) + T_x \tag{2}$$

$$\frac{\partial}{\partial x}(\rho V_x V_y) + \frac{\partial}{\partial y}(\rho V_y V_y) + \frac{\partial}{\partial z}(\rho V_z V_y) = \rho g_y - \frac{\partial P}{\partial y} + \frac{\partial}{\partial x}\left(\mu_e \frac{\partial V_y}{\partial x}\right) + \frac{\partial}{\partial y}\left(\mu_e \frac{\partial V_y}{\partial y}\right) + \frac{\partial}{\partial z}\left(\mu_e \frac{\partial V_y}{\partial z}\right) + T_y \tag{3}$$

$$\frac{\partial}{\partial x}(\rho V_x V_z) + \frac{\partial}{\partial y}(\rho V_y V_z) + \frac{\partial}{\partial z}(\rho V_z V_z) = \rho g_y - \frac{\partial P}{\partial y} + \frac{\partial}{\partial x}\left(\mu_e \frac{\partial V_z}{\partial x}\right) + \frac{\partial}{\partial y}\left(\mu_e \frac{\partial V_z}{\partial y}\right) + \frac{\partial}{\partial z}\left(\mu_e \frac{\partial V_z}{\partial z}\right) + T_z \tag{4}$$

The Turbulent Kinetic Energy (k) and Specific Dissipation Rate (ω) model governs turbulence through the following transport equations:

$$\frac{\partial(\rho k)}{\partial t} + \nabla.(\rho k \vec{u}) = P_k - \beta^* \rho k \omega + \nabla.[(\mu + \sigma_k \mu_t +)\nabla k] \tag{5}$$

$$\frac{\partial \rho \omega}{\partial t} + \nabla.(\rho \omega \vec{u}) = \alpha \frac{\omega}{k} P_k - \beta \rho \omega^2 + \nabla.[(\mu + \sigma_\omega \mu_t)\nabla \omega] + 2(1 - F_1)\rho \sigma_{\omega^2} \frac{1}{\omega} \nabla k.\nabla \omega \tag{6}$$

where ρ denotes fluid density, $u = (v_x, v_y, v_z)$ is the velocity vector, v_x, v_y, and v_z are the velocity components in the x-, y-, and z-directions, respectively, P is the static pressure, $\mu$is the molecular viscosity, μ_t is the turbulent viscosity, and μ_e is the effective viscosity. In addition, P_k represents the production of turbulent kinetic energy, $F_1$is the blending function in the SST formulation, and α, β, β^*, σ_k, and $\sigma_{\omega 2}$ are model constants. Because this study neglects gravitational effects, the body force terms are satisfied $g_x = g_y = g_z = 0$

2.3. Computational Domain and Boundary Conditions

A rectangular computational domain was employed, with the cylinder located at 40% of the streamwise domain length from the inlet (Figure 4). The domain size was 25D x 15D, where D = 40 mm denotes the cylinder diameter. This arrangement provided sufficient downstream space to resolve the wake and recirculation regions. The cylinder center was positioned 10D upstream of the inlet and 15D upstream of the outlet, and it was centered vertically with a 300 mm clearance from both walls.

In the 3-D configuration, the cylinder span was 100 mm, and the domain depth was 200 mm, yielding a wind-tunnel blockage ratio of approximately 2.22%. A velocity inlet and a pressure outlet were imposed at the upstream and downstream boundaries, respectively. For the three-dimensional domain, far-field conditions were applied to the upper and lower boundaries, whereas the side faces were treated as walls. The cylinder surface was specified as a no-slip wall, and the rest of the computational region was assigned as the fluid domain.

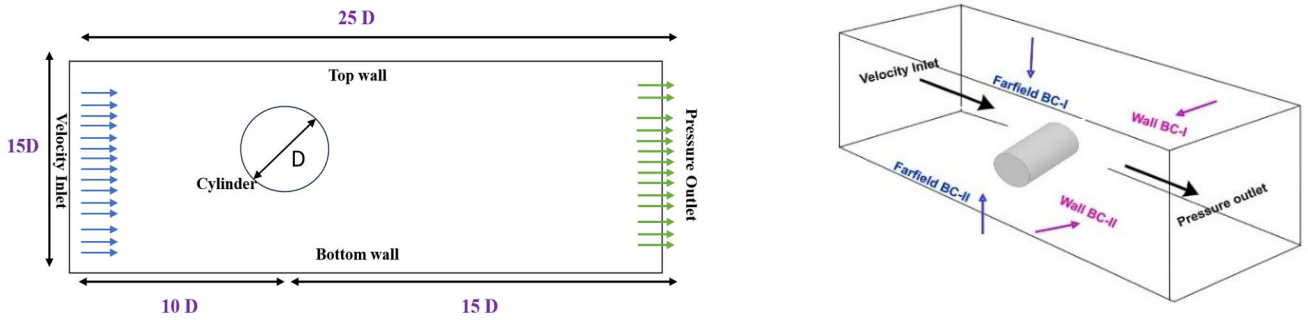

Figure 4. Two-dimensional (2-D) and three-dimensional (3-D) computational domains and boundary conditions.

2.4. Computational Details and Flow Parameters

Computational geometry was generated in ANSYS Design Modeler, and the flow simulations were performed in ANSYS Fluent. A three-dimensional, transient, unsteady Reynolds-averaged Navier-Stokes (URANS) approach was adopted to resolve the unsteady wake dynamics around the cylinder vortex generator configuration. The governing equations were solved using the pressure-based solver, and turbulence closure was provided by the shear stress transport (SST) $k-\omega$ model. This model was selected because it combines the near-wall accuracy of the $k-\omega$ formulation with the free-stream robustness of the $k-\varepsilon$ model and has been shown to perform well in flows with separation and adverse pressure gradients [49].

The Reynolds number is defined as Re = rho U∞ D / mu, where rho is fluid density, U∞ is inlet velocity, D is cylinder diameter, and mu is dynamic viscosity. Vortex shedding is characterized using the Strouhal number St = fD / U∞, where f is the dominant shedding frequency. Pressure-velocity coupling was handled with the SIMPLE algorithm, and second-order spatial discretization was applied to the momentum and turbulence equations. The solution was considered converged when the residuals of all solved equations decreased below the prescribed tolerance. Lift and drag coefficients were obtained by integrating the transverse and streamwise surface forces on the cylinder.

The computational mesh consisted of a triangular-dominant unstructured grid with a characteristic element size of 0.15 mm. To accurately resolve the near-wall flow, 100 inflation layers were applied with a growth rate of 1.25 and a first-layer thickness of 0.1 mm. The mesh was designed to maintain $y^+ \approx 1$, which is appropriate for wall-resolved SST $k-\omega$ simulations. A fixed-time-step approach was employed, and the time-step size was selected to keep the Courant number close to unity. To quantify wake behavior, the recirculation length, Lr/D, was defined as the streamwise distance from the separation point to the downstream location where the mean streamwise velocity recovered to zero. The wake width was defined as the lateral extent of the velocity-deficit region satisfying $u(y) \leq 0.99U_\infty$, while the centerline velocity deficit was calculated as $\Delta U_c(x) = U_\infty - U_c(x)$. For all cases, the vortex generators were installed at an inclination angle of 30° [50].

2.5. Numerical Validation and Mesh-Independence

Numerical benchmarking was first conducted to identify the most suitable turbulence model for the present flow configuration. Predictions obtained using the standard $k-\varepsilon$ and SST $k-\omega$ models were compared with reference experimental data (Figure 5). Although the $k-\varepsilon$ model produced the highest lift-to-drag ratio, it also overpredicted drag more substantially. By contrast, the SST $k-\omega$ model reproduced the reference trend more closely and was therefore selected for all subsequent simulations.

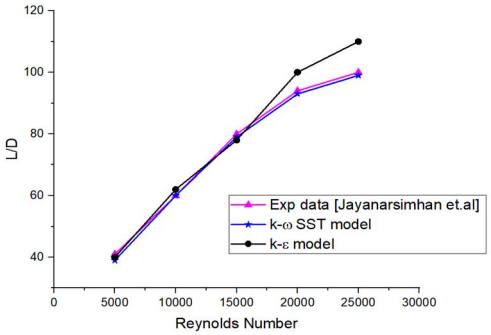

Figure 5. Comparison of the predicted L/D values from the k-ε and SST k-ω models with experimental data over the investigated Reynolds-number range

A mesh-independence study was then performed using three grid levels: coarse, adaptive, and fine (Table 2). Figure 6 shows the variation in the mean lift coefficient with the total number of elements. The adaptive grid was generated using sphere-of-influence refinement around the cylinder, with a minimum local element size of 0.15 mm. The corresponding Strouhal numbers for the course, adaptive, and fine grids were 0.13, 0.17, and 0.20, respectively, indicating that the coarse grid under-resolved the shear-layer roll-up. Because vortex shedding is one of the principal response variables in this study, the fine-grid results were used as the primary reference for interpreting wake dynamics. In contrast, the adaptive grid was retained as a computationally efficient compromise for the parametric comparisons.

Table 2. Results of the grid-dependency study for different mesh resolutions

Grid type	Grid	Elements (x10^6)	$C_{L,\,mean}$	Error (%)	Time (hours)	Strouhal Number
Coarse	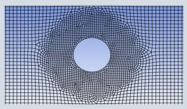	0.68	0.97	~10.9	2.21	0.13
Adaptive	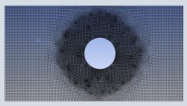	1.02	1.05	~4.50	3.40	0.17
Fully Fine	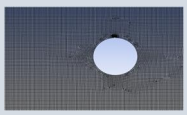	1.98	1.06	~1.8	5.40	0.20

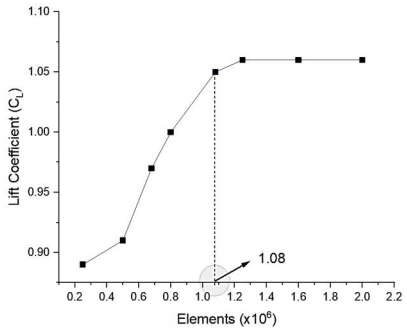

Figure 6. Variation of the mean lift coefficient with the number of mesh elements.

To quantify spatial discretization uncertainty, Richardson extrapolation and the Grid Convergence Index (GCI) were evaluated for C_D, C_L, $C_{L,\mathrm{rms}}$, and St. The resulting GCI values were 3.42% for mean drag, 23.95% for lift fluctuations, and 27.47% for the Strouhal number. These results indicate that mean drag was substantially less sensitive to mesh resolution than the unsteady wake quantities. Accordingly, the wake-related conclusions of this study are presented in comparative terms rather than as absolute high-fidelity spectral predictions.

A time-step independence study was also conducted using three time increments. The corresponding drag coefficients were 1.03, 1.01, and 1.00, while the root-mean-square lift coefficients were 1.25, 1.22, and 1.20, respectively. Because the differences between the two finer time steps were below 3% for all monitored quantities, the intermediate time step was adopted for the remaining analyses. After the initial transients were removed, all flow statistics were averaged over 300 shedding cycles. A running-average assessment further showed that the monitored force and shedding statistics varied by less than 1% over the final 20% of the sampling window.

2.6. Wind Tunnel Analysis

Experimental measurements were conducted in the subsonic wind tunnel at TNPESU to examine the flow past a clean cylinder and cylinders equipped with vortex generators (VGs) (Figure 7a). The wind-tunnel test section measured 300 mm × 600 mm × 1000 mm (Figure 7b). Figure 8 presents the test models, including the clean cylinder and the cylinders fitted with triangular and ogival VGs. The cylinder diameter was selected to satisfy the blockage-ratio requirement of the test section, defined as $B = Acs/Awt$, with $B < 2.22\%$.

The wind-tunnel campaign was conducted with ambient air in a closed test section using a nominal free-stream velocity of approximately 2.5 m/s and an incoming turbulence intensity of about 5%. Because this inflow condition does not fully match the numerical Reynolds number used in the URANS study, the experimental results are used primarily to assess qualitative consistency in the lift-response trends and the relative ranking of the VG cases, rather than as a one-to-one quantitative validation dataset.

(a) (b)

Figure 7. Experimental setup used for wind-tunnel testing at TNPESU: (a) subsonic wind tunnel facility; (b) test section.

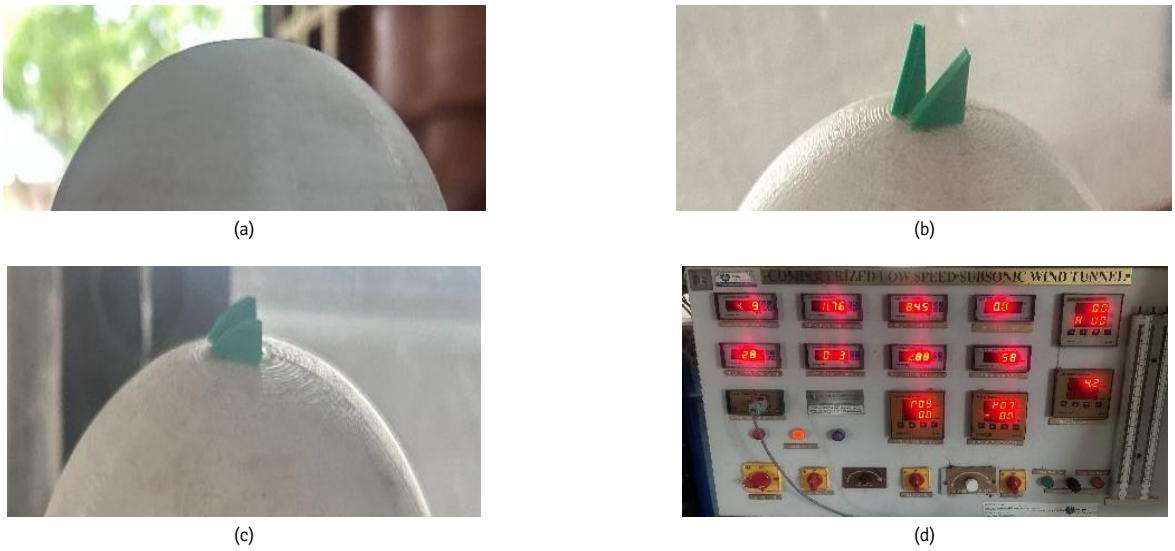

Figure 8. Experimental models and force measurement system: (a) clean cylinder; (b, c) cylinders equipped with triangular and ogival vortex generators, respectively; (d) readout of the force-component balance.

To account for wind-tunnel blockage effects, the measured drag data were corrected using Maskell's bluff-body correction method [51]. The resulting correction was small (approximately 1.2%), indicating that blockage effects were limited for the present setup.

$$C_{D,\infty} = \frac{C_{D,m}}{1 + 0.5ABC_{D,m}} \quad (7)$$

In all test configurations, the vortex generators were mounted at the cylinder apex. Lift and drag forces were measured using a three-component balance installed in the subsonic wind tunnel (Figure 8d).

3. RESULTS

3.1. Velocity Profile

Figures 9 and 10 compare the mean wake structures of the clean cylinder and the VG-equipped configurations. For clarity, the discussion focuses on three quantitative wake indicators, summarized in Table 3: recirculation length, wake width, and centerline velocity deficit. These metrics are used to distinguish local wake contraction from the broader force-response behavior discussed later in the lift section.

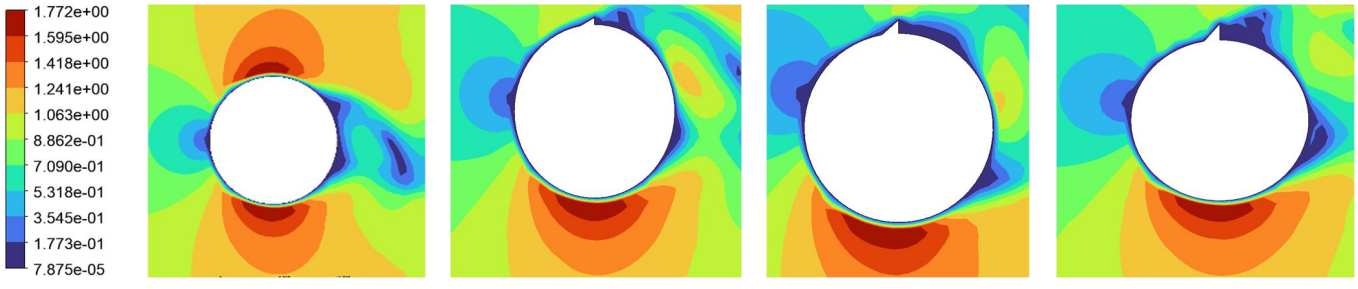

Figure 9. Velocity profile – Clean and cylinder with triangular VGs

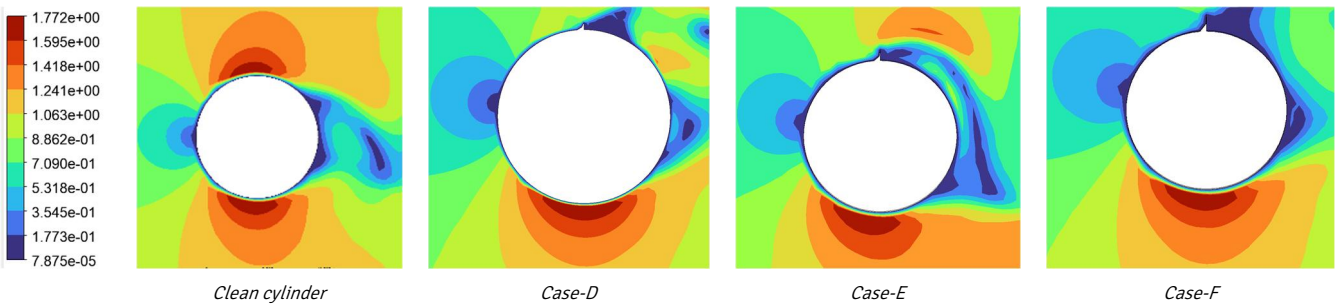

Figure 10. Velocity profile – Clean and cylinder with Ogival VGs

For the triangular VGs (Cases A–C), the wake contracts progressively as the VG height increases. Relative to the clean cylinder, Case A reduces the recirculation length to 1.35D, Case B to 0.90D, and Case C to 0.70D. The same monotonic trend is observed for wake width, which decreases from 1.80D to 1.20D, and for the centerline velocity deficit, which decreases from 0.52 to 0.30. These results indicate that increasing the height of the triangular VGs enhances near-wake contraction and reduces the momentum deficit behind the cylinder.

A similar, although slightly weaker, trend is observed for the ogival VGs (Cases D–F). As the VG height increases, the recirculation length decreases from 1.15D to 0.80D, the wake width from 1.65D to 1.30D, and the centerline velocity deficit from 0.46 to 0.34. Thus, the ogival profile also effectively reorganizes the wake; however, Table 3 shows that, at equal height, the triangular VG produces a somewhat greater reduction in all three wake metrics.

Table 3. Quantitative wake metrics for clean and VG-equipped cylinders

Case	Recirculation Length (L_r/D)	Wake width (W/D)	Centerline velocity deficit ($\Delta U/U_\infty$)
Clean	1.35	1.80	0.52
A	1.10	1.60	0.45
B	0.90	1.40	0.38
C	0.70	1.20	0.30
D	1.15	1.65	0.46
E	0.95	1.45	0.40
F	0.80	1.30	0.34

The main result of Table 3 is therefore twofold. First, all VG configurations improve the wake structure relative to the clean cylinder. Second, the strongest wake contraction is achieved by Case C rather than Case F. This distinction is important because the lift results discussed later show that the configuration yielding the smallest wake metrics is not the same as the one that produces the highest peak lift coefficient. The findings therefore indicate a trade-off between wake suppression and lift enhancement, rather than identifying a single configuration as unequivocally superior across all performance metrics.

3.2. Flow Separation

Flow separation around the clean cylinder is characterized by the formation of separated shear layers on the upper and lower surfaces, followed by the development of alternating vortices in the near wake. When VGs are introduced, the separation topology changes because the streamwise vortices generated near the wall redistribute momentum and alter downstream shear-layer interactions. In the present manuscript, the separation patterns are primarily interpreted from the streamline distributions and near-wake topology (Figures 11–12). Accordingly, the discussion should be regarded as a qualitative comparison unless surface-pressure or wall-shear distributions are incorporated in a revised version.

For the clean cylinder, the wake exhibits the expected broad recirculation region and strong periodic shedding. In Cases A–C, the triangular VGs progressively reduce the size of this separated region, with Case C displaying the most compact wake among the triangular configurations. The streamline patterns are consistent with the quantitative wake metrics reported in Table 3 and suggest that increasing VG height intensifies the modification of the separated shear layers.

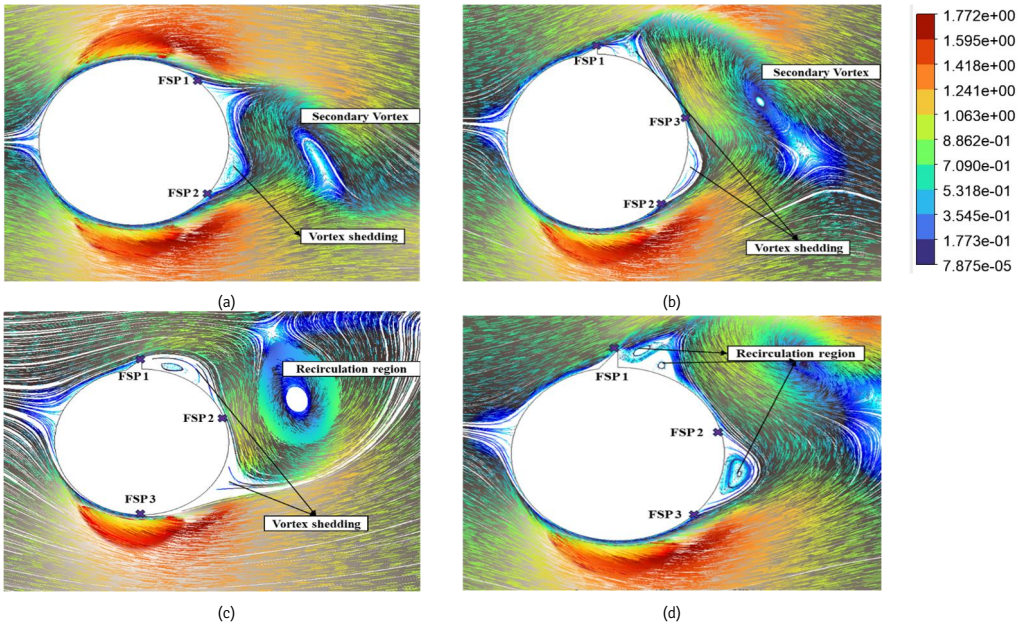

Figure 11. Flow-separation topology for the clean cylinder and triangular-VG: (a) Clean Cylinder (No VGs); (b) Cylinder with VG – Case A; (c) Cylinder with VG – Case B; (d) Cylinder with VG – Case C.

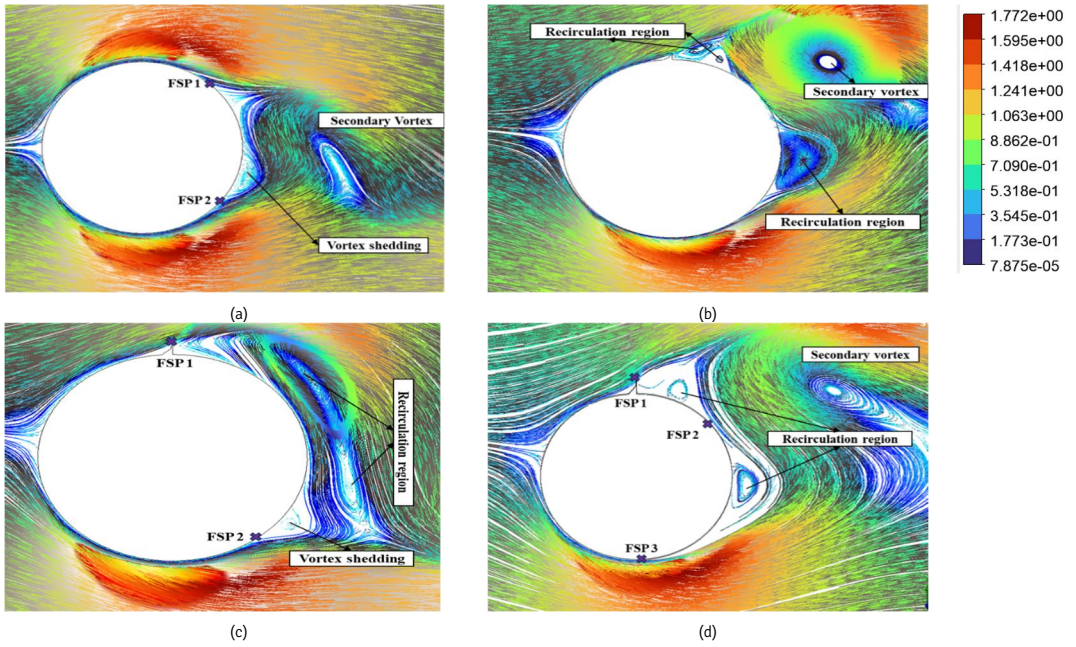

Figure 12. Flow-separation topology for the clean cylinder and ogival-VG: (a) Clean Cylinder (No VGs); (b) Cylinder with VG – Case D; (c) Cylinder with VG – Case E; (d) Cylinder with VG – Case F.

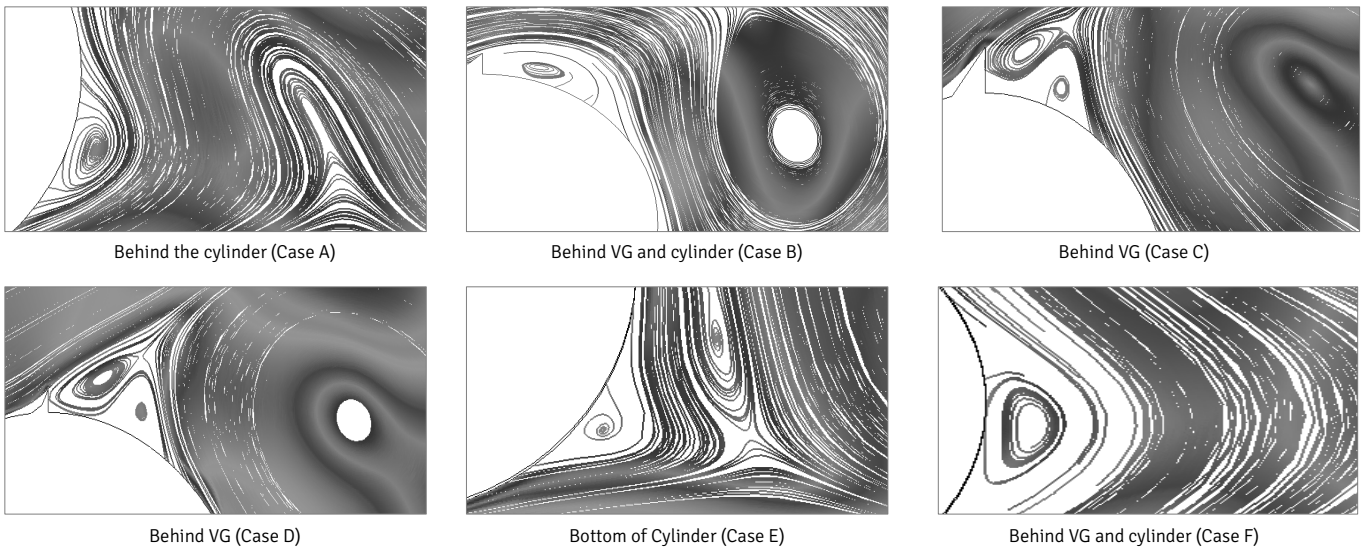

Figure 13. Vortex shedding pattern of cylinder (clean & VG installed)

The ogival cases likewise exhibit a reorganization of the separation structure, although the visual evidence suggests a smoother and more symmetric wake evolution than in the corresponding triangular cases. Any assertion regarding an "additional separation point" or a uniquely optimal topology should therefore be made with caution unless supported by explicit separation-angle measurements or wall-shear distributions. Based on the current evidence, the most defensible conclusion is that the ogival geometry modifies the separation pattern more gradually, whereas the triangular geometry produces stronger near-wake contraction.

From a force-response perspective, the wake visualizations suggest that both VG families reduce the intensity of the separated region relative to the clean cylinder. However, the manuscript should avoid treating streamline plots alone as definitive evidence of drag reduction or spectral content suppression. Reported force coefficients, spectral analyses, or measurements with quantified uncertainty should instead support such claims.

In the numerical benchmark, the clean circular cylinder exhibited classical vortex-shedding behavior, with a Strouhal number close to the canonical subcritical value of approximately 0.20. Because the experimental inflow conditions differed from those used in the numerical setup, the spectral quantities discussed here should be interpreted primarily in relative rather than absolute terms. The main defensible conclusion is that the

VG-equipped cases reduce wake coherence relative to the clean cylinder, with the largest qualitative attenuation observed for the higher-VG configurations.

The flow-separation results suggest that triangular VGs are more aggressive in contracting the wake, whereas ogival VGs produce a smoother redistribution of the separated flow. This distinction helps explain why the configuration yielding the strongest wake contraction is not the same as that producing the highest lift response. These observations should therefore be interpreted as qualitative evidence of flow-structure modification that complements, rather than replaces, the coefficient-based comparison presented in the following sections.

Table 4. Qualitative synthesis of wake and vortex-shedding behavior across the VG cases

Case	Primary flow-control effect	Wake profile	Force-response implication	Recirculation behavior	Vortex-shedding interpretation
Case A	Limited improvement at low VG height	Wake remains relatively wide; contraction versus the clean case is modest	Modest lift increase: force fluctuations remain visible	Reduced relative to the clean case but still pronounced	Periodic shedding persists, though weaker than the baseline
Case B	Moderate triangular-VG control	Narrower and more organized than Case A	Higher lift than Case A with smoother post-peak behavior	Clearly reduced and better controlled	Shedding coherence weakened relative to Case A
Case C	Strongest wake contraction among triangular cases	Most compact wake among triangular configurations	Highest lift among triangular cases	Shortest recirculation region among triangular cases	Shedding is partially suppressed; wake remains structured
Case D	Mild ogival-VG control	More compact and symmetrical than a clean cylinder	Lift improved relative to the clean cylinder	Reduced relative to the clean cylinder	Shedding is weaker and more diffuse than baseline
Case E	Improved ogival control with higher VG	Narrower and smoother wake than Case D	Further lift enhancement with smoother response	More controlled and symmetric	Shedding noticeably weakened
Case F	Highest lift response among ogival cases	Compact and comparatively smooth wake	Highest peak lift among all cases	Short recirculation region, though slightly longer than Case C	Shedding appears least coherent among ogival cases

3.3. Vortex Shedding Characteristics

Vortex shedding from the upper and lower sides of the cylinder produces a low-pressure wake region that generates oscillating lift forces. Table 4 provides a qualitative synthesis of how each configuration modifies the observed shedding pattern, wake compactness, force response, recirculation, and the relative coherence of the wake.

Because Table 4 is qualitative, it should be used only to support the trends already established by the quantitative metrics in Table 3 and the lift curves in Figures 14. The table should not be interpreted as a substitute for quantitative drag, lift-fluctuation, or spectral data. Within that scope, the table supports two consistent trends: increasing VG height improves wake control for both profiles, and the ogival profile—especially Case F—produces the smoothest overall force response, whereas the triangular profile—especially Case C—achieves the strongest local wake contraction.

3.4. Lift Coefficient

For clarity, the abscissa in Figures 13 is interpreted here as the orientation angle of the cylinder–VG assembly relative to the incoming flow. The lift curves obtained from the CFD simulations and experiments are used to assess how wake modifications translate into aerodynamic response. Because the experimental data were not acquired under fully Reynolds-number-matched conditions and uncertainty bars have not yet been reported, the discussion below emphasizes trend consistency and relative case ranking rather than strict numerical agreement.

The clean cylinder exhibits the lowest lift response among all configurations and a pronounced post-peak decline at higher orientation angles. This behavior is associated with early separation and the formation of a broad wake. The experimental results show the same overall pattern, although the exact peak values differ from the CFD predictions, which is not unexpected given the different inflow conditions and the absence of reported measurement uncertainty.

Case A provides a modest improvement over the clean cylinder. Both the CFD and experimental curves indicate a higher peak lift and a slightly delayed post-peak decline, suggesting that even the smallest triangular VG can beneficially modify near-wall momentum transfer. However, the gain remains limited; thus, Case A is best interpreted as a low-intensity control configuration rather than an optimized design.

Case B strengthens this effect. Its lift curve lies above that of Case A over much of the tested angle range, and the post-peak decay is more gradual. This behavior is consistent with the wake metrics reported in Table 3, which show a clear reduction in recirculation length and wake width relative to Case A.

Among the triangular configurations, Case C produces the strongest lift response and the greatest wake contraction. Its higher peak lift, delayed decline, and reduced wake metrics indicate that increasing triangular-VG height enhances both force response and near-wake control within the tested range. Importantly, Case C is the best-performing triangular configuration not only in terms of lift response but also according to the quantitative wake metrics (Table 3).

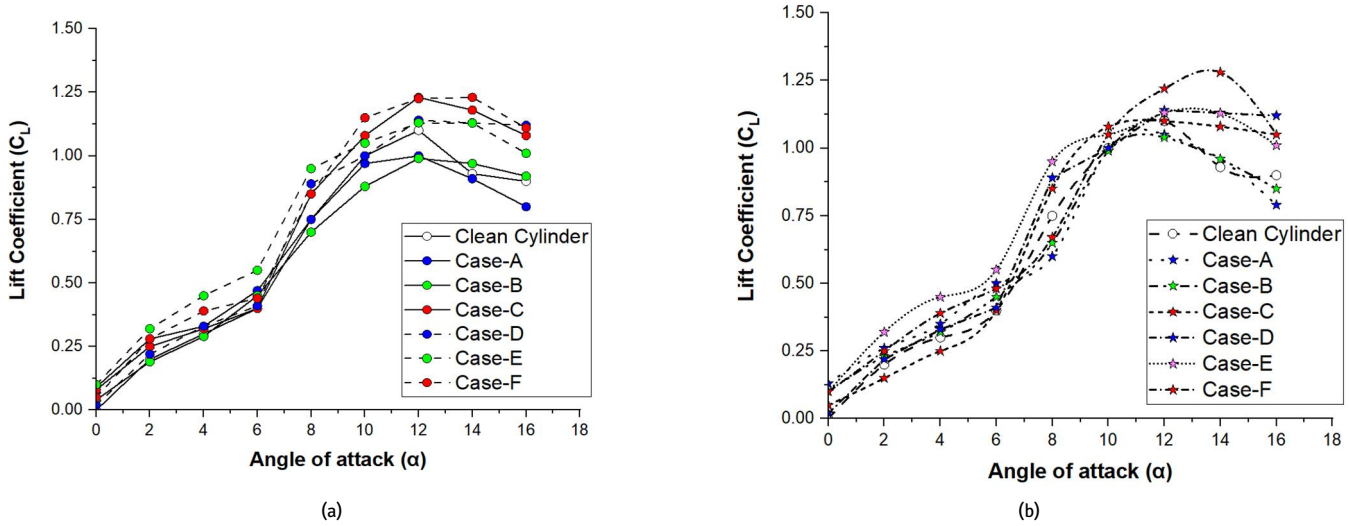

Figure 14. Lift curve comparison of clean cylinder and VG installed cylinders in: (a) CFD analysis, (b) Wind tunnel testing

The ogival configurations continue this progression, but with a different balance between wake suppression and lift generation. Case D improves upon the clean cylinder but does not surpass Case C. Case E further increases the lift response and broadens the range of elevated lift. Case F yields the highest peak lift among all six VG configurations. However, Table 3 shows that its wake contraction remains slightly weaker than that of Case C. The most defensible interpretation, therefore, is not that Case F is universally superior across all metrics, but rather that the ogival geometry is more favorable when the primary objective is to maximize lift under the present test conditions.

Taken together, the lift curves show that both VG profile and height play important roles. Increasing VG height improves performance for both profiles, but the profile shape determines how that improvement is distributed between wake contraction and lift enhancement. The numerical and experimental results are qualitatively consistent in ranking the higher-VG configurations above the lower-VG configurations. Nevertheless, stronger quantitative conclusions should await Reynolds-number-matched experiments with repeated measurements and quantified uncertainty.

4. DISCUSSION

The present findings extend the literature on passive wake control for circular cylinders by showing that vortex-generator (VG) geometry does not improve all aerodynamic outcomes through a single mechanism. Early work by Igarashi [19] showed that VGs mounted on a circular cylinder can modify the Strouhal number, static-pressure distribution, root-mean-square (RMS) pressure fluctuations, and separation location. Similarly, Ünal and Atlar [34] demonstrated using DPIV that streamwise VGs substantially reorganize near-wake topology and alter the characteristic wake length scales of a circular cylinder. More recently, Okbaz et al. [40] reported that VGs reduce velocity fluctuations and drag while modifying the wake and vortex-formation lengths, whereas Aksoy [41] showed that the aerodynamic response of triangular VGs depends strongly on circumferential position and yaw angle. Against this background, the present study provides a more specific comparative insight: although increasing VG height improves wake control for both profiles, the configuration that produces the strongest wake contraction is not the same as that which yields the highest peak lift. Under the present test conditions, the larger triangular VG produces the strongest wake

contraction, whereas the ogival VG at the same height yields the highest lift response. This distinction indicates that wake suppression and lift augmentation should not be regarded as interchangeable performance objectives.

This divergence is physically plausible when interpreted in light of the established operating principle of vortex generators. Huang et al. [52] noted that VGs act by generating streamwise vortices that redistribute momentum and that their effectiveness depends strongly on geometric parameters such as height, width, incidence, and spacing. Li et al. [53] further showed that increasing VG height strengthens vortex intensity and can substantially increase maximum lift, even though not every aerodynamic metric improves in the same way. In the present context, it is therefore reasonable to interpret the stronger wake contraction produced by the taller triangular VGs as the result of stronger local momentum exchange and more forceful restructuring of the separated shear layers. At the same time, the superior lift response of the ogival VG suggests that maximum lift is governed not only by the geometric contraction of the wake, but also by how the VG reshapes the separation pattern and redistributes pressure over the cylinder–VG assembly.

The interpretation that planform exerts an influence independent of height is also consistent with recent studies highlighting the shape sensitivity of VG performance. Wang and Ghaemi [54], [55] showed that nonconventional VG shapes produce distinct three-dimensional wake statistics and coherent structures and further argued that vane shape has a measurable effect on VG performance and momentum transport in the wake. In addition, Palanivel and Mukherjee [56] reported that airfoil-shaped VGs can outperform conventional triangular and rectangular VGs by increasing lift, reducing drag, and generating stronger downstream vorticity in separated blade flow. Although these studies did not examine the exact cylinder configuration considered here, they strongly support the broader interpretation that VG planform should be treated as a primary design variable rather than a secondary geometric detail. From this perspective, the present results are physically consistent: the sharper triangular VG appears to be more effective at compressing the wake, whereas the smoother ogival VG appears to promote a pressure-field reorganization that is more favorable for lift generation.

The present wake and lift trends also refine the interpretation of recent cylinder-specific VG studies. In the work of Okbaz et al. [40], drag reduction was strongly correlated with wake and vortex-formation length scales, which helps explain why wake modification is often treated as a key control metric. However, Aksoy [41] demonstrated that even within triangular-VG configurations, changes in circumferential position and yaw angle can substantially alter the measured response. Considered together with the present findings, these results point to an important conclusion: a configuration that is optimal in terms of wake contraction is not necessarily optimal in terms of peak lift. The present data therefore argue against using wake narrowing alone as a universal surrogate for overall aerodynamic improvement.

The discussion should nevertheless remain consistent with the evidential limits of the present study. First, although the wind-tunnel measurements exhibit qualitatively similar lift trends, the experimental inflow speed differs from that used in the numerical simulations; accordingly, the agreement should be interpreted as support for the observed trends rather than as strict quantitative validation. Second, unsteady quantities such as $C_{L,\mathrm{rms}}$ and the Strouhal number are generally more sensitive to mesh and temporal resolution than mean quantities, which suggests that any claim regarding spectral suppression should be made with appropriate caution. Third, only one VG placement and one inclination angle were examined; therefore, the triangular–ogival trade-off identified here should not yet be generalized to a broader design space without further evidence. These limitations do not diminish the central contribution of the study, but they do define the conditions under which its conclusions should be interpreted.

Within these limits, the most defensible design implication is that triangular VGs are more suitable when the primary objective is stronger local wake contraction, whereas ogival VGs are more attractive when peak lift enhancement is prioritized under the present operating conditions. This interpretation is also consistent with the broader VG literature, in which Huang et al. [52] and Li et al. [53] emphasized that VG effectiveness depends on the interaction among multiple geometric variables rather than on any single parameter. More broadly, the present results support treating passive appendage design for bluff bodies as a multi-objective optimization problem. Future work should therefore combine Reynolds-number-matched experiments, repeated force measurements with quantified uncertainty, and higher-fidelity diagnostics, such as surface-pressure measurements, phase-averaged PIV, or scale-resolving simulations, to determine whether the observed trade-off is driven primarily by differences in vortex formation, pressure redistribution, or attenuation of wake coherence.

5. CONCLUSION

This study compared a clean circular cylinder with cylinders fitted with triangular and ogival vortex generators of three heights using transient URANS simulations and supporting wind-tunnel measurements. Relative to the baseline cylinder, all VG configurations improved the wake and force response by reducing the recirculation region, narrowing the wake, and increasing lift over part of the tested angle range.

The results reveal a consistent profile-dependent trade-off. Case C (triangular, 10 mm) produced the strongest wake contraction, whereas Case F (ogival, 10

mm) achieved the highest maximum lift coefficient. Accordingly, the configuration that most strongly suppresses the wake is not identical to the configuration that maximizes lift. Under the present test conditions, ogival VGs appear promising for lift enhancement, while triangular VGs remain attractive for stronger wake contraction. These conclusions should nevertheless be interpreted within the limits of the present numerical resolution and the non-matched experimental inflow conditions.

ACKNOWLEDGMENTS
The authors would like to express their deepest gratitude to the University and laboratory support (wind-tunnel components) that facilitated the successful completion of this research.

CONFLICTS OF INTEREST
The authors declare that no conflicts of interest are associated with this study. All aspects of the research were conducted with the utmost integrity and transparency.

DATA AVAILABILITY
The datasets utilized and analyzed during this research are available from the corresponding author upon reasonable request.

ETHICAL STATEMENTS
Not applicable. This study did not involve any human participants or animals, and no personal or sensitive data were collected, used, or analyzed at any stage of the research.

FUNDING
This research was conducted without financial support. The authors confirm that no funding was received for this study's research, analysis, or publication.

REFERENCES

[1] B. L. Storms and C. S. Jang, "Lift enhancement of an airfoil using a Gurney flap and vortex generators," J. Aircr., vol. 31, no. 3, pp. 542–547, 1994, https://doi.org/10.2514/3.46528

[2] B. Gardarin, L. Jacquin, and P. Geffroy, "Flow separation control with vortex generators," in 4th AIAA Flow Control Conference, 2008, p. 3773. https://doi.org/10.2514/6.2008-3773

[3] D. Baldacchino, C. Ferreira, D. De Tavernier, W. A. Timmer, and G. J. W. van Bussel, "Experimental parameter study for passive vortex generators on a 30% thick airfoil," Wind Energy, vol. 21, no. 9, pp. 745–765, 2018, https://doi.org/10.1002/we.2191

[4] W. J. Crowther, M. Jabbal, and S. C. Liddle, "Flow control fallacies: A review of commonpitfalls in flow control research," Proc. Inst. Mech. Eng. Part G J. Aerosp. Eng., vol. 225, no. 1, pp. 1–11, 2011, https://doi.org/10.1243/09544100JAERO761

[5] S. Lee et al., "A Review of Flow Control Strategies for Supersonic/Hypersonic Fluid Dynamics," Aerosp. Res. Commun., vol. 2, p. 13149, 2024, https://doi.org/10.3389/arc.2024.13149

[6] J. Wang et al., "Low Drag Automotive Mirrors Using Passive Jet Flow Control," SAE Int. J. Passeng. Cars - Mech. Syst., vol. 7, no. 2, pp. 538–549, 2014, https://doi.org/10.4271/2014-01-0584

[7] M. J. Bloxham and J. P. Bons, "A global approach to turbomachinery flow control: Passage vortex control," J. Turbomach., vol. 136, no. 4, p. 41003, 2013, https://doi.org/10.1115/1.4024686

[8] M. G. De Giorgi, F. Marra, E. Pescini, and A. Ficarella, "Experimental and numerical analysis of a micro plasma actuator for active flow control in turbomachinery," in Proceedings of the ASME Turbo Expo, 2014, vol. 2A, p. V02AT37A011. https://doi.org/10.1115/GT2014-25337

[9] H. Hatoum and L. P. Dasi, "Reduction of Pressure Gradient and Turbulence Using Vortex Generators in Prosthetic Heart Valves," Ann. Biomed. Eng., vol. 47, no. 1, pp. 85–96, 2019, https://doi.org/10.1007/s10439-018-02128-6

[10] J. B. R. Rose, S. G. Natarajan, and V. T. Gopinathan, "Biomimetic flow control techniques for aerospace applications: a comprehensive review," Rev. Environ. Sci. Biotechnol., vol. 20, no. 3, pp. 645–677, 2021, https://doi.org/10.1007/s11157-021-09583-z

[11] T. R. Johnson and P. N. Joubert, "The influence of vortex generators on the drag and heat transfer from a circular cylinder normal to an airstream," J. Heat Transfer, vol. 91, no. 1, pp. 91–99, 1969, https://doi.org/10.1115/1.3580126

[12] M. Saleem, A. Karnam, O. Rodriguez, J. Liu, and E. Gutmark, "Flow and acoustic fields investigation of noise reduction by micro vortex generators in supersonic nozzles," Phys. Fluids, vol. 35, no. 10, 2023, https://doi.org/10.1063/5.0170104

[13] T. Igarashi, "Effect of Tripping Wires on the Flow Around a Circular Cylinder Normal To an Airstream.," Bull. JSME, vol. 29, no. 255, pp. 2917–2924, 1986, https://doi.org/10.1299/jsme1958.29.2917

[14] R. M. J. Groh and J. Croll, "Towards Tolerance Specifications for the Elastic Buckling Design of Axially Loaded Cylinders," J. Appl. Mech. Trans. ASME, vol. 91, no. 1, p. 11004, 2024, https://doi.org/10.1115/1.4063032

[15] D. C. McCormick, "Boundary layer separation control with directed synthetic jets," in 38th Aerospace Sciences Meeting and Exhibit, 2000, p. 519. https://doi.org/10.2514/6.2000-519

[16] M. Abdollahzadeh, J. C. Pascoa, and P. J. Oliveira, "Comparison of DBD plasma actuators flow control authority in different modes of actuation," Aerosp. Sci. Technol., vol. 78, pp. 183–196, 2018, https://doi.org/10.1016/j.ast.2018.04.013

[17] K. Jayanarasimhan and N. K. Balasubramanian, "Passive flow control in wind turbine blade by geometrical optimization of vortex generator," in E3S Web of Conferences, 2023, vol. 399, p. 3006. https://doi.org/10.1051/e3sconf/202339903006

[18] K. S. Choi, "Smart flow control with riblets," Adv. Mater. Res., vol. 745, pp. 27–40, 2013, https://doi.org/10.4028/www.scientific.net/AMR.745.27

[19] T. Igarashi, "Effect of Vortex Generators on the Flow Around a Circular Cylinder Normal To an Airstream.," in Bulletin of the JSME, 1985, vol. 28, no. 236, pp. 274–282. https://doi.org/10.1299/jsme1958.28.274

[20] D. Shiels, A. Leonard, and A. Roshko, "Flow-induced vibration of a circular cylinder at limiting structural

parameters," J. Food Compos. Anal., vol. 15, no. 1, pp. 3–21, 2002.

[21] H. C. Lim and S. J. Lee, "Flow control of a circular cylinder with O-rings," Fluid Dyn. Res., vol. 35, no. 2, pp. 107–122, 2004, https://doi.org/10.1016/j.fluiddyn.2004.05.001

[22] J. Wang and Y. Zhao, "Heat and fluid flow characteristics of a rectangular channel with a small diameter circular cylinder as vortex generator," Int. J. Therm. Sci., vol. 92, pp. 1–13, 2015, https://doi.org/10.1016/j.ijthermalsci.2015.01.018

[23] A. Izhar, A. H. Qureshi, and S. Khushnood, "Simulation of vortex-induced vibrations of a cylinder using ANSYS CFX rigid body solver," China Ocean Eng., vol. 31, no. 1, pp. 79–90, 2017, https://doi.org/10.1007/s13344-017-0010-9

[24] H. Yu, W. L. Chen, H. Li, F. Auteri, and D. Gao, "Control of cylinder wake dynamics with symmetric synthetic jets near the flow separation points," Exp. Fluids, vol. 67, no. 2, p. 16, 2026, https://doi.org/10.1007/s00348-026-04171-9

[25] H. Jiang, "Separation angle for flow past a circular cylinder in the subcritical regime," Phys. Fluids, vol. 32, no. 1, 2020, https://doi.org/10.1063/1.5139479

[26] A. K. Soti and A. De, "Vortex-induced vibrations of a confined circular cylinder for efficient flow power extraction," Phys. Fluids, vol. 32, no. 3, 2020, https://doi.org/10.1063/1.5131334

[27] M. Chatzimanolakis, P. Weber, and P. Koumoutsakos, "Vortex separation cascades in simulations of the planar flow past an impulsively started cylinder up to," J. Fluid Mech., vol. 953, p. R2, 2022, https://doi.org/10.1017/jfm.2022.988

[28] M. Gong and B. Dally, "Dynamic response of a cylinder-plate-cylinder system coupling wake-induced and interference effects," Phys. Fluids, vol. 37, no. 10, 2025, https://doi.org/10.1063/5.0289251

[29] B. Li, Y. Li, and T. Li, "Numerical investigation on the flow past circular cylinders with modification of partially covered V-shaped riblets in the subcritical regime using large eddy simulation," Phys. Fluids, vol. 38, no. 2, 2026, https://doi.org/10.1063/5.0311108

[30] U. Fernandez-Gamiz, I. Errasti, R. Gutierrez-Amo, A. Boyano, and O. Barambones, "Computational modelling of rectangular sub-boundary layer vortex generators," Appl. Sci., vol. 8, no. 1, p. 138, 2018, https://doi.org/10.3390/app8010138

[31] H. D. Taylor, "Design Criteria For And Applications Of The Vortex Generator Mixing Principal," National Advisory Committee for Aeronautics, 1948. [Online]. Available: https://ntrs.nasa.gov/api/citations/19680068324/downloads/19680068324_Update.pdf

[32] G. W. Gyatt, "Development and testing of vortex generators for small horizontal axis wind turbines," AeroVironment, Inc., Monrovia, CA (USA), 1986. [Online]. Available: http://www.osti.gov/energycitations/product.biblio.jsp?osti_id=6801076

[33] M. Kobayashi and H. Maekawa, "Turbulent flow accompanied by Taylor-Goertler vortices in a two-dimensional curved channel," Flow Meas. Instrum., vol. 6, no. 2, pp. 93–100, 1995.

[34] U. O. Ünal and M. Atlar, "An experimental investigation into the effect of vortex generators on the near-wake flow of a circular cylinder," Exp. Fluids, vol. 48, no. 6, pp. 1059–1079, 2010, https://doi.org/10.1007/s00348-009-0791-6

[35] A. Aziz, Y. Zhang, and C. Gang, "Computational Studies of Passive Vortex Generators for Flow Control on High-Speed Train," in Sustainable Civil Infrastructures, 2021, vol. Part 32, pp. 95–108. https://doi.org/10.1007/978-3-030-79641-9_7

[36] K. Jayanarasimhan and N. K. Balasubramanian, "An overview of flow control in aerodynamic surfaces using vortex generators," Phys. Fluids, vol. 37, no. 3, 2025, https://doi.org/10.1063/5.0260937

[37] N. K. Balasubramanian, K. Jayanarasimhan, M. Nagaraj, and M. Sivasankari, "Computational Optimization of Flow Control over Aircraft Wing Section using Vortex Generators," Int. J. Adv. Sci. Eng., vol. 12, no. 1, pp. 5007–5016, 2025, https://doi.org/10.29294/IJASE.12.1.2025.5007-5016

[38] M. T. Baissi, A. Brima, K. Aoues, R. Khanniche, and N. Moummi, "Thermal behavior in a solar air heater channel roughened with delta-shaped vortex generators," Appl. Therm. Eng., vol. 165, p. 113563, 2020, https://doi.org/10.1016/j.applthermaleng.2019.03.134

[39] R. Maouedj, Y. Menni, M. Inc, Y. M. Chu, H. Ameur, and G. Lorenzini, "Simulating the Turbulent Hydrothermal Behavior of Oil/MWCNT Nanofluid in a Solar Channel Heat Exchanger Equipped with Vortex Generators," C. - Comput. Model. Eng. Sci., vol. 126, no. 3, pp. 855–889, 2021, https://doi.org/10.32604/cmes.2021.014524

[40] A. Okbaz, M. H. Aksoy, N. Kurtulmuş, and A. B. Çolak, "Flow control over a circular cylinder using vortex generators: Particle image velocimetry analysis and machine-learning-based prediction of flow characteristics," Ocean Eng., vol. 288, p. 116055, 2023, https://doi.org/10.1016/j.oceaneng.2023.116055

[41] M. H. Aksoy, "Flow characteristics and passive flow control of circular cylinders with triangular vortex generators: An experimental investigation," Appl. Ocean Res., vol. 142, p. 103836, 2024, https://doi.org/10.1016/j.apor.2023.103836

[42] Y. Wang, J. Wang, W. Zhang, and Z. Zhao, "Performance optimization of plate-fin heat exchanger with curved vortex generators based on response surface method," Int. J. Therm. Sci., vol. 210, p. 109659, 2025, https://doi.org/10.1016/j.ijthermalsci.2024.109659

[43] S. Muddada and B. S. V. Patnaik, "An active flow control strategy for the suppression of vortex structures behind a circular cylinder," Eur. J. Mech. B/Fluids, vol. 29, no. 2, pp. 93–104, 2010, https://doi.org/10.1016/j.euromechflu.2009.11.002

[44] J. C. Schulmeister, J. M. Dahl, G. D. Weymouth, and M. S. Triantafyllou, "Flow control with rotating cylinders," J. Fluid Mech., vol. 825, pp. 743–763, 2017, https://doi.org/10.1017/jfm.2017.395

[45] A. Jirásek, "Vortex-generator model and its application to flow control," J. Aircr., vol. 42, no. 6, pp. 1486–1491, 2005, https://doi.org/10.2514/1.12220

[46] M. L. Shur, M. K. Strelets, A. K. Travin, and P. R. Spalart, "Evaluation of vortex generators for separation control in a transcritical cylinder flow," AIAA J., vol. 53, no. 10, pp. 2967–2977, 2015, https://doi.org/10.2514/1.J053851

[47] D. Heine, K. Ehrenfried, G. Heine, and S. Huntgeburth, "Experimental and theoretical study of the pressure wave generation in railway tunnels with vented tunnel

portals," J. Wind Eng. Ind. Aerodyn., vol. 176, pp. 290–300, 2018, https://doi.org/10.1016/j.jweia.2018.03.020

[48] M. Matejka, P. Pick, J. Nozicka, and P. Prochazka, "Experimental study of influence of active methods of flow control on the flow field past a cylinder," J. Flow Vis. Image Process., vol. 16, no. 4, pp. 353–366, 2009, https://doi.org/10.1615/JFlowVisImageProc.v16.i4.60

[49] F. R. Menter, "Two-equation eddy-viscosity turbulence models for engineering applications," AIAA J., vol. 32, no. 8, pp. 1598–1605, 1994, https://doi.org/10.2514/3.12149

[50] F. R. Menter, M. Kuntz, and R. Langtry, "Ten Years of Industrial Experience with the SST Turbulence Model Turbulence heat and mass transfer," Cfd.Spbstu.Ru, vol. 4, no. July 2014, pp. 625–632, 2003, [Online]. Available: http://cfd.mace.manchester.ac.uk/flomania/pds_papers/file_pds-1068134610Menter-SST-paper.pdf

[51] E. C. Maskell, "A Theory of Blockage Effects on Bulff Bodies and Stalled Wings in a Closed Wind Tunnel," London, United Kingdom, 1965. [Online]. Available: https://reports.aerade.cranfield.ac.uk/handle/1826.2/3982

[52] Y. X. Huang, P. H. Chung, K. M. Chung, and C. Y. Huang, "Downstream influence of turbulent flow past vortex generators," J. Mech., vol. 39, pp. 471–479, 2023, https://doi.org/10.1093/jom/ufad039

[53] X. K. Li, W. Liu, T. J. Zhang, P. M. Wang, and X. D. Wang, "Experimental and numerical analysis of the effect of vortex generator installation angle on flow separation control," Energies, vol. 12, no. 23, p. 959, 2019, https://doi.org/10.3390/en12234583

[54] S. Wang and S. Ghaemi, "Effect of vane sweep angle on vortex generator wake," Exp. Fluids, vol. 60, no. 1, p. 24, 2019, https://doi.org/10.1007/s00348-018-2666-1

[55] S. Wang and S. Ghaemi, "Three-dimensional wake of nonconventional vortex generators," AIAA J., vol. 57, no. 3, pp. 949–961, 2019, https://doi.org/10.2514/1.J057420

[56] H. Palanivel and R. Mukherjee, "Airfoil-shaped vortex generators for separation control and drag reduction on wind turbine blades," Acta Mech., vol. 235, no. 12, pp. 7765–7787, 2024, https://doi.org/10.1007/s00707-024-04126-3